Check for updates

Geophysical Research Letters

RESEARCH LETTER
10.1029/2024GL108140

Supersaturation and Critical Size of Cloud Condensation Nuclei in Marine Stratus Clouds

Henrik Svensmark[1], Martin Bødker Enghoff[1], Jacob Svensmark[2], Irina Thaler[3], and Nir J. Shaviv[3]

[1]DTU Space, Technical University of Denmark, Lyngby, Denmark, [2]Atmospheric, Oceanic and Planetary Physics, Department of Physics, University of Oxford, Oxford, UK, [3]Racah Institute of Physics, Hebrew University of Jerusalem, Jerusalem, Israel

Key Points:

- On average, supersaturation in marine clouds is significantly higher than the conventional view of 0.2%–0.3%
- Due to the higher supersaturation, much smaller aerosols get activated into cloud droplets
- The results are essential for better understanding aerosols-cloud interactions

Supporting Information:

Supporting Information may be found in the online version of this article.

Correspondence to:

H. Svensmark,
hsv@space.dtu.dk

Citation:

Svensmark, H., Enghoff, M. B., Svensmark, J., Thaler, I., & Shaviv, N. J. (2024). Supersaturation and critical size of cloud condensation nuclei in marine stratus clouds. *Geophysical Research Letters*, *51*, e2024GL108140. https://doi.org/10.1029/2024GL108140

Received 18 NOV 2023
Accepted 23 MAR 2024

Author Contributions:

Formal analysis: Henrik Svensmark
Investigation: Henrik Svensmark
Software: Henrik Svensmark
Validation: Martin Bødker Enghoff, Jacob Svensmark, Irina Thaler, Nir J. Shaviv
Writing – original draft: Henrik Svensmark
Writing – review & editing: Henrik Svensmark, Martin Bødker Enghoff, Jacob Svensmark, Irina Thaler, Nir J. Shaviv

© 2024. The Authors.
This is an open access article under the terms of the Creative Commons Attribution License, which permits use, distribution and reproduction in any medium, provided the original work is properly cited.

Abstract Observations of marine stratus clouds in clean air off the Californian coast reveal a functional relationship between the number of cloud condensation nuclei (CCN) and supersaturation. Satellite-derived liquid droplet density estimates the number density of CCN. Combining the estimated supersaturation using Köhler theory, global maps of supersaturation and the critical activation size of CCN are estimated. Here, we show that high supersaturation >0.5% persists over the oceans with a critical CCN size of 25–30 nm, which is smaller than the conventional wisdom of 60 nm. Independent support for such high supersaturation in the marine cloud is obtained from CCN measurements provided by the "Atmospheric Tomography Mission." Higher supersaturation implies smaller activation size for CCN making cloud formation more sensitive to changes in aerosol nucleation.

Plain Language Summary Clouds in Earth's atmosphere are of fundamental importance for the climate by regulating the reflection of sunlight into space and interacting with thermal radiation from Earth. Clouds form when moist air ascends and gets supersaturated with water vapor that condenses on aerosol particles of sufficient sizes, which then grow into cloud droplets. The aerosol number-density and size spectrum influence the resulting cloud properties, and the supersaturation determines which aerosols can be activated into cloud drops. Here, we show that the supersaturation in marine liquid clouds is significantly higher than in the conventional view. As a consequence, much smaller aerosols can serve as cloud condensation nuclei. This can make cloud formation more sensitive to changes in aerosol properties than previously thought. Such a result should be of general interest and lead to a better understanding of aerosol-cloud interactions, which presently constitute the largest uncertainty in our understanding of climate.

1. Introduction

Clouds are an essential part of Earth's climate system. At the same time, clouds constitute one of the largest uncertainties in our understanding of climate change. Clouds cool the planet by ∼20 W m^{-2} (Loeb et al., 2009), which is around five times more than the heating from the doubling of CO_2. Thus, small changes in cloud properties accompanying anthropogenic activity may amplify or dampen that warming. In fact, the IPCC report lists aerosol-cloud-forcing feedback as the largest source of uncertainty in Earth's radiation budget (Masson-Delmotte et al., 2021).

In supersaturated air, aerosols larger than a critical size can function as cloud condensation nuclei (CCN), upon which water vapor condenses, thus transforming these particles into cloud droplets. The number density of activated CCN determines cloud micro-physics, such as droplet density, optical thickness, and liquid water path (LWP). These parameters control the amount of solar energy that reaches Earth's surface and the amount of thermal energy radiated back to space. Generally accepted wisdom sets the typical critical CCN size to ∼60 nm (Fan et al., 2018; Hegg et al., 2009) or higher (Pierce & Adams, 2009), corresponding to supersaturation levels of typically 0.2%–0.3% (Hoppel et al., 1985, 1990; Boucher et al., 2013, Sect. 7.3.3.3). Observations of clouds off the Californian coast showed that supersaturations often exceeded 1% in clean marine air (Hudson & Noble, 2014; Hudson et al., 2010). These observations suggest that much smaller particles than those set by conventional estimates can nucleate stratus cloud droplets.

The presence of small aerosol particles in the atmosphere is well documented. For example, nucleation of new aerosols (∼1 nm) in marine areas often happens in the free troposphere/lower stratosphere (Williamson

19448007, 2024, 9, Downloaded from https://agupubs.onlinelibrary.wiley.com/doi/10.1029/2024GL108140 by Royal Danish Library, Wiley Online Library on [10/06/2024]. See the Terms and Conditions (https://onlinelibrary.wiley.com/terms-and-conditions) on Wiley Online Library for rules of use; OA articles are governed by the applicable Creative Commons License

et al., 2019, 2021), and the aerosols grow during descent. There are also several observations of nucleation mode aerosols in the tropical marine boundary layer (Clarke et al., 1998) and the subtropical Pacific boundary layer (Petters et al., 2006), while a large Aitken mode (>100 cm^{-3} and 10–80 nm) was found below the clouds in the southeast Pacific (Terai et al., 2014; Wood et al., 2008). This work examines the global consequence of higher supersaturation on the activation of CCN into cloud drops.

An association between supersaturation and droplet concentration can be expected from basic principles. The supersaturation in a cloud with a uniform updraft velocity increases as the air cools adiabatically. However, supersaturation causes the water vapor to condense on the growing water droplets, depleting the water vapor concentration and weakening the supersaturation. Therefore, a lower droplet concentration (N_c) results in a smaller loss of the available water vapor and a larger supersaturation.

By exploring a relationship between satellite-determined liquid droplet concentrations and supersaturation, it is possible using Köhler theory to obtain a global estimate of the critical size (s) of CCN (Petters & Kreidenweis, 2007). One consequence of having smaller critical CCN sizes is that the gas-to-particle nucleation and growth are more important to the cloud formation process. The reason is that the probability of a small aerosol surviving to a small-sized CCN is much larger, thus making the amount of CCN more sensitive to changes in nucleation and growth rates.

2. Materials and Methods

2.1. Linear Regression and Confidence Intervals

A linear regression fit is given to the data points $x_i = N_{1\%}$ (the amount of CCN at 1% supersaturation (S)) and $y_i = \log_{10} S_{\text{eff}}$, which provides a regression line, $y = \tilde{\alpha}x + \tilde{\beta}$. The measured points are scattered around this line, as shown in Figure 1a. Confidence lines are given by

$$y_{\pm 90\%}(x) = \tilde{\alpha}x + \tilde{\beta} \pm t_{\alpha/2,n-2}\sigma\sqrt{1 + \frac{1}{n} + \frac{(x-\bar{x})^2}{S_{xx}}} \tag{1}$$

here $t_{\alpha/2,n-2} = 1.292$ is the one-sided t-distribution for 90% confidence, n is the number of observation points (83 points), x is the independent variable, $\bar{x}$ is the mean of the number density $N_{1\%}$, and finally, $S_{xx} = \sum_i (x_i - \bar{x})^2$ is the variance of the density $N_{1\%}$, and

$$\sigma = \sqrt{\frac{\sum_i \left(y_i - (\alpha x_i + \beta)\right)}{n-2}} \tag{2}$$

The confidence ±90% lines can be seen in Figure 1a as the two dashed lines.

2.2. Droplet Concentration From τ, LWP, r_e, and Cloud Fraction C_f

The droplet concentration (N_c) as a function of liquid water path (LWP) and cloud optical thickness (τ) can be remotely sensed by satellite (Bennartz, 2007)

$$N_c = \left(\frac{5^3}{3^5 2^{3/2}\pi}\right) k^{-1} c_w^{1/2} \rho^2 \, \tau^3 \, (\text{LWP})^{-5/2}. \tag{3}$$

where ρ is the density of water, c_w is the condensation rate of water and $k = (r_v/r_e)^3$ (the ratio between the volume radius r_v and effective radius r_e), and defined in Supporting Information S1 to be 0.8. In the case of satellite observations where LWP is estimated in a given pixel area, it is necessary to scale LWP with the cloud fraction C_f, that is, LWP = $> \frac{LWP}{C_f}$, since part of the pixel area may be cloud free, therefore (Bennartz, 2007)

$$N_c = \left(\frac{5^3}{3^5 2^{3/2}\pi}\right) k^{-1} c_w^{1/2} \rho^2 \, \tau^3 \left(\frac{\text{LWP}}{C_f}\right)^{-5/2}. \tag{4}$$

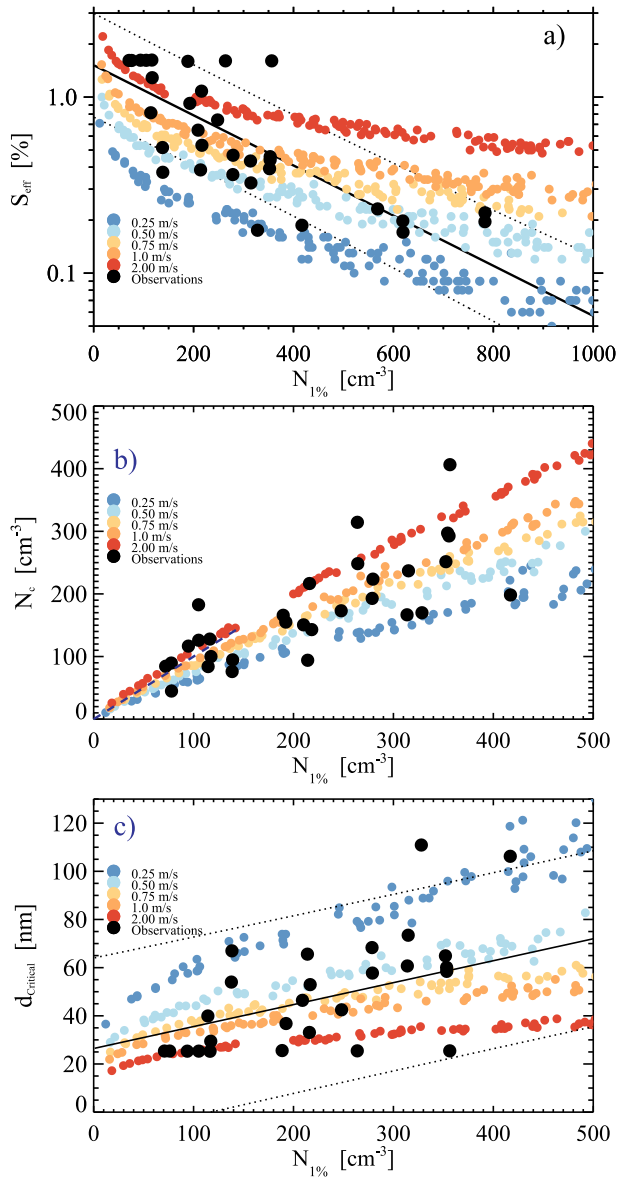

Figure 1. Top panel (a) The effective supersaturation S_{eff} as a function of $N_{1\%}$ based on airborne observations (black circles from Hudson and Noble (2014)). The solid, dashed black line is a linear regression to the data. The dashed lines are 90% confidence intervals (see Methods). The colored circular symbols are modeled maximum supersaturation in a cloud as a function of $N_{1\%}$ for five updraft velocities. The Middle panel (b) Modeled droplet number density N_c activated at a given vertical velocity as a function of $N_{1\%}$, a measure of the total number of cloud condensation nuclei at 1% supersaturation, is shown as the colored circular symbols. Black circular points are observations of Hudson and Noble (2014). Bottom panel (c) is the critical activation diameter d_{critical} as a function of $N_{1\%}$. The colored circular symbols are the modeled critical diameters as a function of vertical velocity and $N_{1\%}$. Circular black symbols are Köhler theory applied to the measured supersaturation as a function of $N_{1\%}$. The solid, dashed black line is a linear regression to the data. The dashed lines are 90% confidence intervals (see Methods).

Using Moderate Resolution Imaging Spectroradiometer (MODIS) data, and ρ = 1,000 kg/m^3 and $C_f \geq$ [0.7, 0.8, 0.9], we can calculate the geographical distribution of N_c (For a detailed derivation, see Supporting Information S1).

3. Results

3.1. Supersaturation and Droplet Concentration of Marine Stratus Clouds

Hudson et al. (2010) and Hudson and Noble (2014) used several airborne observations of clouds outside the Californian coast from which a simple relation between supersaturation and the number density of CCN, $N_{1\%}$, can be derived. Figure 1a depicts the measurements from the Physics of Stratocumulus Top (POST) (Carman et al., 2012) campaign as black circles, similar to Figure 13c of Hudson and Noble (2014). Note how the effective supersaturation S_{eff} decreases with $N_{1\%}$, the number of CCN (1% supersaturation is used in the measurements to activate most CCN). Note that POST was sampled in both clean and polluted maritime air. A simple linear regression using the observations, $N_{1\%}$ and $\log_{10}S_{\text{eff}}$ as independent and dependent variables, provide the following functional relation

$$S_{\text{eff}} = \alpha \exp(-\beta N_{1\%}), \tag{5}$$

with $\alpha = 1.51^{+0.26}_{-0.21}$ % and $\beta = 0.0033^{+0.0005}_{-0.0004}$ cm^3 (2σ). The two dashed lines in Figure 1a are 90% confidence intervals (see methods).

This functional fit will be used to estimate the global marine supersaturation and, thereby, the critical size (s) of CCN over the oceans.

3.2. Droplet Growth by Condensation

It is of interest to compare the observations with numerical simulations of cloud droplet activation using the "pyrcel" zero-dimensional, adiabatic cloud parcel model (Rothenberg & Wang, 2016, see https://pyrcel.readthedocs.io/en/latest/index.html).

This model makes it possible to calculate the change in supersaturation as the air ascends with a constant velocity (Rothenberg & Wang, 2016). The maximum supersaturation S_{max} in a cloud determines the number of cloud droplets activated, N_c, from the marine aerosol distribution. The modeled marine aerosol distributions are the sum of three log-normal distributions

$$n(r) = \sum_{i=1}^{3} \frac{c_i N_i}{\sqrt{2\pi}\log\sigma_i} \exp\left(-\frac{\log^2(r/\mu_i)}{2\log^2\sigma_i}\right), \tag{6}$$

$\log_{10}\sigma_i$ = [0.657, 0.210, 0.396], μ_i = [0.0039, 0.133, 0.2] μm and N_i = [133.00, 10.00, 1.06] cm^{-3}. Where $c_i = c$ [α_i, β_i, γ_i] are stochastic parameters, and [α_i, β_i, γ_i] are drawn from lognormal distributions ($\mu = 0$ and $\sigma = 0.25$), and c is an increasing parameter. The number of droplets, N_c, activated in each run is found for a predetermined vertical velocity and stochastic c_i. To connect with the observations, $N_{1\%}$ is calculated by reusing the c_i in Equation 6 and finding a vertical velocity for which the maximal supersaturation is 1%. The number of droplets activated is then $N_{1\%}$. The initial air temperature is 274 K, and a hygroscopicity parameter κ of 0.72, a typical value in clean marine air (Andreae & Rosenfeld, 2008; Schulze et al., 2020), and with a pressure of 800 hPa appropriate for low liquid clouds. Figure 1a

19448007, 2024, 9, Downloaded from https://agupubs.onlinelibrary.wiley.com/doi/10.1029/2024GL108140 by Royal Danish Library, Wiley Online Library on [10/06/2024]. See the Terms and Conditions (https://onlinelibrary.wiley.com/terms-and-conditions) on Wiley Online Library for rules of use; OA articles are governed by the applicable Creative Commons License

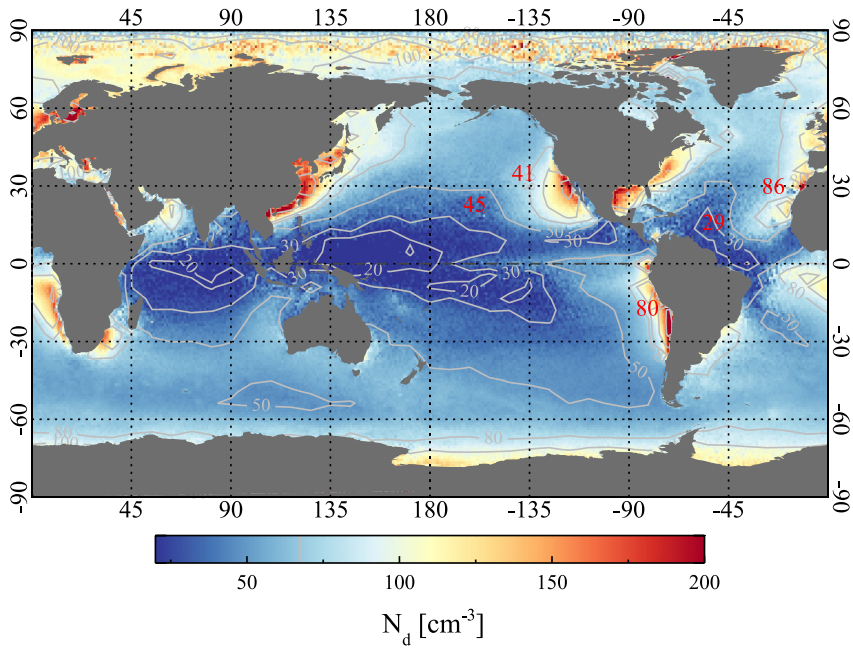

Figure 2. Liquid cloud droplet concentration based on Moderate Resolution Imaging Spectroradiometer observations of optical thickness and liquid water path averaged over the period 2003.1.3–2021.12.31. The average droplet density is $N_{\text{average}} = 58.9\ \text{cm}^{-3}$, which agrees with previous estimates (Grosvenor et al., 2018).

displays the model calculations of maximum supersaturations as colored circular symbols as a function of $N_{1\%}$ and for five velocities of ascent (see labels).

Figure 1b shows the number of activated cloud droplets, N_c, as a function of $N_{1\%}$ for five different vertical velocities (see labels). Note the abscissa axis is restricted to $N_{1\%} = [0.500]$, reflecting clean marine air. The black circles in Figure 1b are based on airborne observations of marine stratus cumulus clouds of the Pacific coast of California (data from Hudson et al. (2010) and Hudson and Noble (2014)).

Figure 1c depicts the critical size of activated CCN as a function of five different vertical velocities and $N_{1\%}$. The black circles are the critical sizes found by inserting observed supersaturation S_{eff} shown in Figure 1a, into Equation 7 (replacing Equation 5 with S_{eff}), describing how aerosols activate as CCN using Köhler theory.

3.3. Droplet Concentration of Marine Warm Liquid Clouds

We will now employ satellite observations to estimate the droplet density of low, warm clouds over the oceans. The cloud droplet density can then be used to estimate supersaturation over the oceans, from which Köhler theory makes it possible to calculate the critical CCN sizes.

Droplet concentration N_c in marine warm clouds can be calculated using the cloud optical thickness τ and LWP LWP (Bennartz, 2007), both of which can be retrieved from satellite observations, using Equation 4 together with the cloud optical thickness, LWP, and cloud fraction obtained from the MODIS and averaged over the period 2003.1.3–2021.12.31, resulting in the global droplet density distribution. The temperature at the cloud base is approximated by adding 4.5 K (1 km cloud thickness with a typical wet adiabatic lapse rate) to the cloud top temperature. This is used to calculate the condensation rate c_w. In the estimate of the droplet density N_c, a threshold cloud fraction is applied to the pixels (Bennartz, 2007). Three threshold values were used to test the robustness $C_f \geq [0.7, 0.8, 0.9]$. Two values are larger than 0.7 used in Bennartz (2007), resulting in slightly larger droplet concentrations (see Table S1 in Supporting Information S1).

Figure 2 depicts the global climatology of marine warm cloud droplet concentration using a cloud fraction threshold of $C_f > 0.9$. Observe that the droplet concentration is typically below 100 cm^{-3} and, in large areas, even lower than 50 droplets cm^{-3} (see supplementary material for maps of thresholds 0.7, 0.8). Shown in red on the map are the cloud droplet concentrations from in situ observations: VOCALS ($N_c = 80\ \text{cm}^{-3}$) (Bretherton

19448007, 2024, 9, Downloaded from https://agupubs.onlinelibrary.wiley.com/doi/10.1029/2024GL108140 by Royal Danish Library, Wiley Online Library on [10/06/2024]. See the Terms and Conditions (https://onlinelibrary.wiley.com/terms-and-conditions) on Wiley Online Library for rules of use; OA articles are governed by the applicable Creative Commons License

et al., 2010), FIRE ($N_c = 41$ cm^{-3}) (Yum & Hudson, 2002), Hawaii ($N_c = 45$ cm^{-3}) (Jiusto, 1967), NARVAL-II ($N_c = 29$ cm^{-3}) (Wolf et al., 2019, average of Table 4), and ASTEX ($N_c = 86$ cm^{-3}) (Yum & Hudson, 2002). Note that this result does not apply when other cloud types are dominant.

3.4. Global Critical Diameter of CCN in Marine Stratus

With the cloud supersaturation as a function of $N_{1\%}$ (Equation 5), it is possible to estimate the critical diameter at which aerosols activate as CCN by using Köhler theory. Inserting Equation 5 for the supersaturation S in the Köhler expression for the critical diameter one gets (Petters & Kreidenweis, 2007),

$$d_{\text{critical}} = \left(\frac{4A^3}{27\kappa \log^2[\alpha \exp(-\beta N_{1\%})]}\right)^{1/3}. \quad (7)$$

where κ is the hygroscopicity parameter related to different solutes, for example, for sulfuric acid $\kappa \sim 0.9$, $A = 0.6/T$ [μm], T is temperature, and $N_{1\%}$ is the number of CCN at 1% supersaturation. $N_{1\%}$ can be related to N_c as follows. In clean marine air with low cloud droplet numbers, it is not dynamics via the vertical velocity, W, which dominates the droplet number N_c. This can be seen from Figure 1b where effectively the simulations show that $N_c \propto N_{1\%} \sim N_{\text{CCN}}$ in the limit $N_c \to 0$ and independent of the vertical velocity. An analytic expression where $N_c \propto N_{\text{CCN}}^{\frac{2}{k'+2}} W^{\frac{3k'}{2k'+4}}$ supports this result (Twomey, 1977), here k' is a real positive parameter, which can be found as the log-log slope of cumulative N_{CCN} with S. If $k' \ll 1$ leads effectively to $N_c \propto N_{\text{CCN}}$, which is an approximate proportionality observed in clean marine environments (Hudson et al., 2010; Martin et al., 1994). The model results shown in Figure 1b give $k' = 0.26$ corresponding to $\frac{2}{k'+2} \sim 0.9$ and $\frac{3k'}{2k'+4} \sim 0.2$, which is close to the values of k' from the observations of Hudson and Noble (2014, Figure 1b) at supersaturation $\gtrapprox 0.5\%$. Therefore $N_{1\%} \approx N_c^{(1.0/0.9)}$ will be used in Equation 7.

Since naturally formed aerosols contain several different substances, the hygroscopic parameter κ is a weighted average of constituents. Estimates of the hygroscopic parameter κ of aerosols in the marine boundary layer over the Pacific give a $\kappa = 0.72$ for clean marine air and for air that is a mixture of marine air and continental air $\kappa = 0.41$ (Andreae & Rosenfeld, 2008; Schulze et al., 2020). Here, we are mainly concerned with clean marine air except near continental coasts, and $\kappa = 0.72$ will be preferred (Table S1 in Supporting Information S1 shows that the changes to the critical diameter are relatively small by using, e.g. $\kappa = 0.41$ instead).

Using Köhler theory, Equation 7 and the global droplet distribution, we obtain the spatial distribution of critical CCN sizes in low marine clouds, as shown in Figure 3a. Figure 3b shows the corresponding supersaturations. As a conservative estimate of the critical diameter, Figure 3c is based on the lower bound of the 90% confidence interval (see Methods), meaning that 90% of measurements of the critical diameter should be larger than the estimates shown in the map. Figure 3d is the corresponding supersaturations.

It is essential to see if results independent of Hudson et al. (2010) and Hudson and Noble (2014) can support higher supersaturations. We use data from the Atmospheric Tomography Mission (ATom) to test this (Brock et al., 2022). ATom was a global-scale atmosphere aircraft sampling mission, profiling worldwide from 0.2 to 12 km altitude in the four seasons between 2016 and 2018. Figure 4c shows the flight passes. Of relevance here was air sampled at supersaturations 0.1%, 0.2%, 0.5%, and 1% to obtain the number densities of CCN. Importantly, Hudson and Noble's (2014) measurements were from just below the clouds. Therefore, to test the Hudson and Noble (2014) results, the ATom data were sorted according to the measured humidity (RH), assuming that when RH increases toward 100%, the measurements are near or within clouds. Figure 4a is the CCN density as a function of altitude at 0.5% supersaturation without restrictions on humidity. The red points are 1 km binned averages with one standard deviation. Figure 4b is similar to Figure 4a, but all measurements have RH >75%. Notice that the distribution shifts toward lower CCN number densities. Finally, Figure 4d shows the average (1 km < altitude < 8 km) CCN number density as a function of RH discrimination and for supersaturations of 1%, 0.5%, 0.2% and 0.1%. The green diamond symbols are for measurements where RH is larger than the RH value on the abscissa, and the orange triangular symbols are for humidity RH in bins of 10%. The red circle at 100% humidity denotes the average droplet density $N_{\text{average}} = 58.9$ cm^{-3} obtained from Figure 2.

19448007, 2024, 9, Downloaded from https://agupubs.onlinelibrary.wiley.com/doi/10.1029/2024GL108140 by Royal Danish Library, Wiley Online Library on [10/06/2024]. See the Terms and Conditions (https://onlinelibrary.wiley.com/terms-and-conditions) on Wiley Online Library for rules of use; OA articles are governed by the applicable Creative Commons License

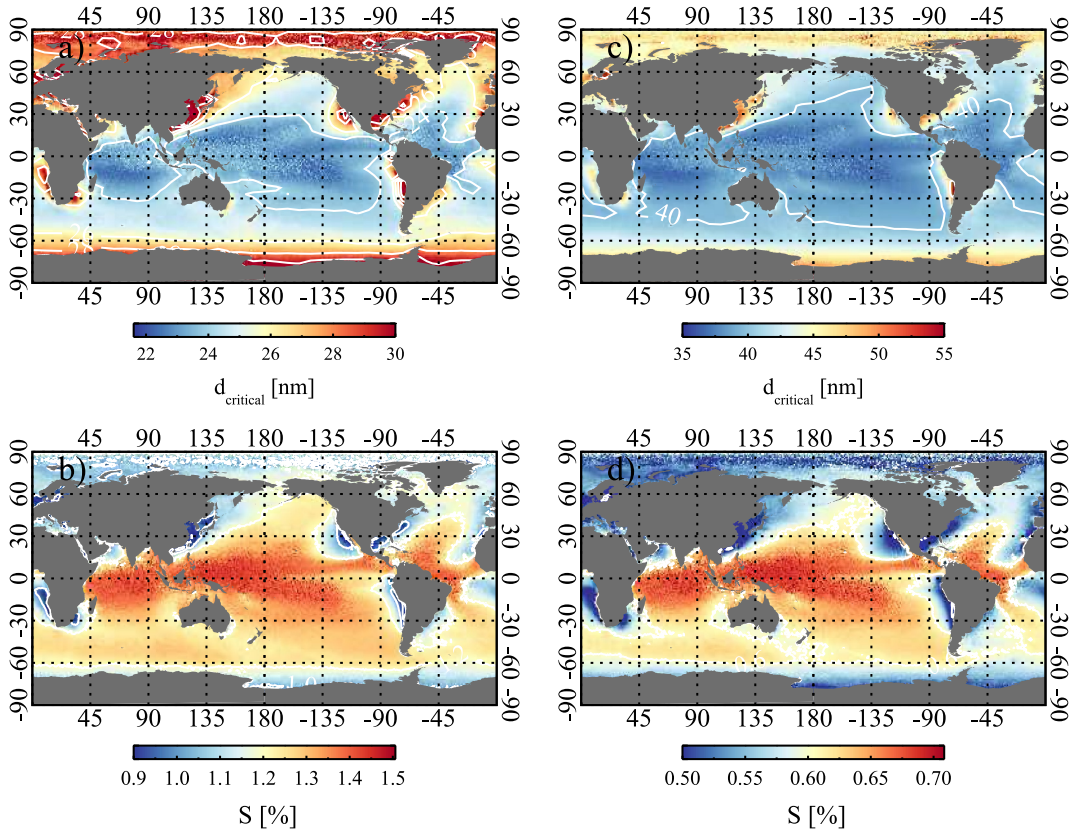

Figure 3. Global distribution of critical cloud condensation nuclei (CCN) sizes and supersaturation in low marine clouds. (a) Map of the critical CCN diameter based on the regression line in Figure 1 that relates the cloud droplet concentration to cloud supersaturation, and finally Köhler theory, Equation 7, for the critical CCN diameter (mean diameter 24.9 nm). (b) A map of the corresponding effective supersaturation (mean supersaturation 1.25%). (c) As (a) but using the lower bound of the 90% confidence interval to give the critical CCN's maximal sizes (mean diameter 40.2 nm), and (d) The corresponding supersaturation (mean supersaturation 0.6%). Using $\kappa = 0.72$ for clean marine air with a cloud fraction threshold is $C_f > 0.9$.

4. Discussion

Observations by Hudson et al. (2010) and Hudson and Noble (2014) suggest that the supersaturation in marine stratus clouds increases as the droplet number decreases. In the cleanest air, the supersaturation may exceed 1%, activating small critical CCN, as shown in Figure 1a. The modeled supersaturation as a function of $N_{1\%}$ shown in Figure 1b as the colored curves conform broadly with the observations with vertical velocities in the range 0.25–2.0 m/s. Although the vertical velocity inside marine stratus clouds averaged over a long horizontal path should be close to zero due to ascending and descending velocities, there are regions of maximum ascending velocities where the smallest CCN activate due to higher supersaturation levels. Typical maximum vertical velocities of accent, measured in marine stratocumulus clouds, are 1–2 m/s and somewhat lower in marine stratus clouds (Zheng et al., 2016).

Hudson et al. (2010) and Hudson and Noble (2014)'s observations of the relation between droplet density and supersaturation, seen in Figure 1, make it possible to obtain an empirical relation between droplet number density and supersaturation in marine stratus clouds as given by Equation 5 globally. The lowest droplet concentrations are just outside the range of observations in Figure 1. It is not surprising since the data in Figure 1 was measured relatively close to the Californian coast, and air may be mixed with continental air, which elevates the CCN density. In contrast, one finds very low droplet concentrations in remote oceans (Jiusto, 1967; Wolf et al., 2019; Yum & Hudson, 2002). The extrapolation needed in Figure 1 to encompass low droplet concentrations is straightforward and is supported by the numerical simulations.

High supersaturations ($S > 0.5\%$) in marine clouds differ from the conventional view that the supersaturation is ~ 0.2%–0.3%. Measurements of CCN in marine air using S ~0.2% typically result in a low CCN density in

19448007, 2024, 9, Downloaded from https://agupubs.onlinelibrary.wiley.com/doi/10.1029/2024GL108140 by Royal Danish Library, Wiley Online Library on [10/06/2024]. See the Terms and Conditions (https://onlinelibrary.wiley.com/terms-and-conditions) on Wiley Online Library for rules of use; OA articles are governed by the applicable Creative Commons License

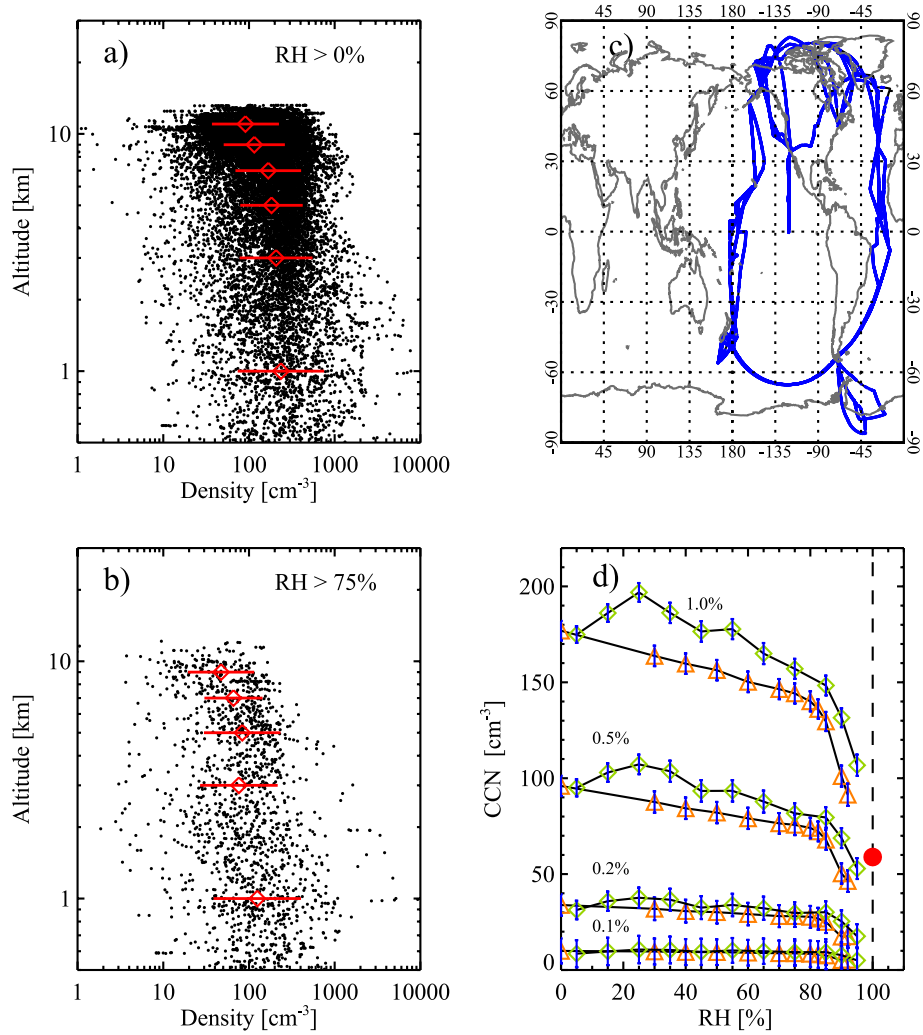

Figure 4. Panel (a) The number density of cloud condensation nuclei (CCN) measured at a supersaturation of 0.5% based on observations from the Atmospheric Tomography Mission (ATom) as a function of the altitude of measurements where the humidity (measured humidity (RH)) > 0%. The red points are averages based on binned altitude in intervals of 2 km. Panel (b) is the same as (a), but for RH > 75%. Panel (c) displays the longitude and latitude of the ATom flight passes. Panel (d) shows the average CCN number density (1–9 km) as a function of RH at supersaturation 1%, 0.5%, 0.2%, and 0.1%. The green diamond symbols are measurements for which the humidity is larger than an RH threshold (given by the value on the RH-axis), and the orange triangular symbols are measurements where the RH is a binned interval of 10%.

agreement with the observed low droplet density. In contrast, measurements using ∼0.8% give a too-high CCN density higher than the observed droplet number density and appear at odds with high supersaturations. This discrepancy can be clarified using the ATom measurements of CCN density using supersaturations of 0.1%, 0.2%, 0.5%, and 1%. The measurements in Hudson and Noble (2014) were from just below the clouds; therefore, the ATom CCN densities are combined with simultaneous measurements of humidity RH, assuming that humidity → 100% reflects the proximity of clouds. Figures 4a and 4b show the CCN density at 0.5% supersaturation and RH > 0% and RH > 75%, obtained along the ATom flight paths shown in Figure 4c. Measurement of CCN at supersaturations 0.1%, 0.2%, 0.5%, and 1% is demonstrated in Figure 4d as a function of the humidity. As the measurements advance toward clouds (RH → 100%), the number density of CCN in all cases decreases. The red circular symbol at 100% humidity is the average cloud droplet density over the oceans, and it is seen from Figure 4d that the supersaturations must be >∼0.5% to reproduce this droplet number. This limit fits well with the results of Hudson et al. (2010) and Hudson and Noble (2014). The observed decrease in CCN density as RH → 100% is not entirely understood and might be related to scavenging by rain or drizzle or, in some cases, cloud processing. Notably, these ATom measurements do not determine clouds or cloud types.

19448007, 2024, 9, Downloaded from https://agupubs.onlinelibrary.wiley.com/doi/10.1029/2024GL108140 by Royal Danish Library, Wiley Online Library on [10/06/2024]. See the Terms and Conditions (https://onlinelibrary.wiley.com/terms-and-conditions) on Wiley Online Library for rules of use; OA articles are governed by the applicable Creative Commons License

19448007, 2024, 9, Downloaded from https://agupubs.onlinelibrary.wiley.com/doi/10.1029/2024GL108140 by Royal Danish Library, Wiley Online Library on [10/06/2024]. See the Terms and Conditions (https://onlinelibrary.wiley.com/terms-and-conditions) on Wiley Online Library for rules of use; OA articles are governed by the applicable Creative Commons License

The data are mainly over the oceans and a restricted altitude of 0.5–9 km. Performing the same analysis with the altitude restricted to 0.5–4 km does not change the conclusions. Therefore, the suggestion is that high supersaturations are a relatively general feature of marine liquid clouds in clean air.

Combining Köhler theory with global satellite retrieved liquid droplet number density, the critical size of CCN is obtained. Figure 3a shows that sizes between 20 and 30 nm activate over the remote oceans and from Figure 3b that the corresponding supersaturations are of the order 1%. Correspondingly, Figures 3c and 3d demonstrate with 90% confidence that the critical size measurements should be smaller than ∼40 nm and the supersaturation larger than 0.6%. In all cases, the activation sizes are significantly smaller than the conventional sizes of ∼60 nm. A test of the robustness of the results was performed using three cloud thresholds $C_f \geq [0.7, 0.8, 0.9]$ and simultaneously varying the parameters α and β in the relation between droplet density (N_c) and supersaturation (S) seen in Equation 5. Table S1 in Supporting Information S1 shows the effect in d_{critical} for a 2σ variation on α and β and three cloud thresholds. One finds a relative change in d_{critical} of ∼20%, demonstrating the robustness of the results (see Supporting Information S1 for maps of d_{critical}).

5. Conclusion

In conclusion, the critical activation sizes of aerosols in clean marine stratus clouds are 25–30 nm and much smaller than the generally accepted size of about 60 nm. Such small CCN sizes result from high supersaturations in the range of 0.5%–1.0% and get support from observations and modeling studies. In situ, ATom measurements of CCN densities at supersaturations 0.1%, 0.2%, 0.5%, and 1% near clouds also support low CCN number density at supersaturation between 0.5% and 1.0%. Therefore, the Atom data provides consistency between the model results and cloud observations of high supersaturations and low cloud droplet numbers in clean marine air. One noteworthy consequence of having a smaller critical CCN size is that aerosol particles nucleated directly from the gas phase are less likely to be scavenged by larger aerosols before they reach a critical CCN size as they have to grow less and thus more aerosols will be available for activation into cloud drops. Consequently, variations in gas-to-particle nucleation and growth to CCN are more important for cloud formation than previously thought. This, of course, only applies if activation happens quickly, and thus, the result should only be seen as an increased potential for variations in aerosol nucleation to affect cloud formation. Significantly higher supersaturations should be consequential in understanding and modeling cloud processes.

Data Availability Statement

The empirical relation between cloud droplet density and supersaturation is based on data from Hudson and Noble (2014) Figure 13. Satellite observations of clouds are obtained from the "MODIS" (MODIS) data over the period 2003.1.3–2021.12.31. The version of MODIS data used is MOD08_D3 - MODIS/Terra Aerosol Cloud Water Vapor Ozone Daily L3 Global 1Deg CMG. Data can be downloaded from [https://ladsweb.modaps.eosdis.nasa.gov/archive/allData/61/MOD08_D3/]. Measured CCN densities at various supersaturations used in this study are from the Atmospheric Tomography Mission (ATom) (Brock et al., 2022) [https://doi.org/10.3334/ORNLDAAC/2111] using the data files: [ATom_60s_aerosol_data.nc] and [ATom_aerosol_profiles.nc]. Data files on critical CCN sizes and supersaturation used to produce Figure 3 in this study are provided as supplementary files and are available in Dryad [https://doi.org/10.5061/dryad.cnp5hqccr].

Acknowledgments
HS acknowledges the support of a Lady Davis visiting professorship during a stay at the Hebrew University of Jerusalem, Israel. We thank the referees for their helpful suggestions. JS is supported by the Carlsberg Foundation.

References

Andreae, M., & Rosenfeld, D. (2008). Aerosol–cloud–precipitation interactions. Part 1. The nature and sources of cloud-active aerosols. *Earth-Science Reviews*, *89*(1), 13–41. https://doi.org/10.1016/j.earscirev.2008.03.001

Bennartz, R. (2007). Global assessment of marine boundary layer cloud droplet number concentration from satellite. *Journal of Geophysical Research*, *112*(D2), D02201. https://doi.org/10.1029/2006JD007547

Boucher, O., Randall, D., Artaxo, P., Bretherton, C., Feingold, G., Forster, P., et al. (2013). Clouds and aerosols. In T. F. Stocker, D. Qin, G.-K. Plattner, M. Tignor, S. K. Allen, J. Boschung, et al. (Eds.), *Climate change 2013: The physical science basis. Contribution Of Working Group I to the Fifth Assessment Report of the Intergovernmental Panel on Climate Change (chap. 7)*. Cambridge University Press.

Bretherton, C. S., Wood, R., George, R. C., Leon, D., Allen, G., & Zheng, X. (2010). Southeast Pacific stratocumulus clouds, precipitation and boundary layer structure sampled along 20° S during VOCALS-REx. *Atmospheric Chemistry and Physics*, *10*(21), 10639–10654. https://doi.org/10.5194/acp-10-10639-2010

Brock, C., Froyd, K., Dollner, M., Williamson, C., Schill, G., Murphy, D., et al. (2022). *ATom: Comprehensive aerosol properties, 2016–2018, version 2*. ORNL Distributed Active Archive Center. https://doi.org/10.3334/ORNLDAAC/2111

Carman, J. K., Rossiter, D. L., Khelif, D., Jonsson, H. H., Faloona, I. C., & Chuang, P. Y. (2012). Observational constraints on entrainment and the entrainment interface layer in stratocumulus. *Atmospheric Chemistry and Physics*, *12*(22), 11135–11152. https://doi.org/10.5194/acp-12-11135-2012

Clarke, D., Davis, A. D., Kapustin, V. N., Eisele, F., Chen, G., Paluch, I., et al. (1998). Particle nucleation in the tropical boundary layer and its coupling to marine sulfur sources. *Science*, *282*(5386), 89–92. https://doi.org/10.1126/science.282.5386.89

Fan, J., Rosenfeld, D., Zhang, Y., Giangrande, S. E., Li, Z., Machado, L. A. T., et al. (2018). Substantial convection and precipitation enhancements by ultrafine aerosol particles. *Science*, *359*(6374), 411–418. https://doi.org/10.1126/science.aan8461

Grosvenor, D. P., Sourdeval, O., Zuidema, P., Ackerman, A., Alexandrov, M. D., Bennartz, R., et al. (2018). Remote sensing of droplet number concentration in warm clouds: A review of the current state of knowledge and perspectives. *Reviews of Geophysics*, *56*(2), 409–453. https://doi.org/10.1029/2017RG000593

Hegg, D. A., Covert, D. S., Jonsson, H. H., & Woods, R. (2009). Differentiating natural and anthropogenic cloud condensation nuclei in the California coastal zone. *Tellus B: Chemical and Physical Meteorology*, *61*(4), 669–676. https://doi.org/10.1111/j.1600-0889.2009.00435.x

Hoppel, W., Fitzgerald, J., Frick, G., Larson, R. E., & Mack, E. J. (1990). Aerosol size distributions and optical properties found in the marine boundary layer over the Atlantic Ocean. *Journal of Geophysical Research*, *95*(D4), 3659–3686. https://doi.org/10.1029/JD095iD04p03659

Hoppel, W., Fitzgerald, J., & Larson, R. (1985). Aerosol size distributions in air masses advecting off the East Coast of the United States. *Journal of Geophysical Research*, *90*(D1), 2365–2379. https://doi.org/10.1029/JD090iD01p02365

Hudson, J. G., & Noble, S. (2014). CCN and vertical velocity influences on droplet concentrations and supersaturations in clean and polluted stratus clouds. *Journal of the Atmospheric Sciences*, *71*(1), 312–331. https://doi.org/10.1175/JAS-D-13-086.1

Hudson, J. G., Noble, S., & Jha, V. (2010). Stratus cloud supersaturations. *Geophysical Research Letters*, *37*(21), L21813. https://doi.org/10.1029/2010GL045197

Jiusto, J. E. (1967). Aerosol and cloud microphysics measurements in Hawaii. *Tellus*, *19*(3), 359–368. https://doi.org/10.1111/j.2153-3490.1967.tb01491.x

Loeb, N. G., Wielicki, B. A., Doelling, D. R., Smith, G. L., Keyes, D. F., Kato, S., et al. (2009). Toward optimal closure of the Earth's top-of-atmosphere radiation budget. *Journal of Climate*, *22*(3), 748–766. https://doi.org/10.1175/2008jcli2637.1

Martin, G. M., Johnson, D. W., & Spice, A. (1994). The measurement and parameterization of effective radius of droplets in warm stratocumulus clouds. *Journal of the Atmospheric Sciences*, *51*(13), 1823–1842. https://doi.org/10.1175/1520-0469(1994)051⟨1823:TMAPOE⟩2.0.CO;2

Masson-Delmotte, V., Zhai, P., Pirani, A., Connors, S. L., Péan, C., Berger, S., et al. (2021). *Climate change 2021: The physical science basis*. IPCC.

Petters, M. D., & Kreidenweis, S. M. (2007). A single parameter representation of hygroscopic growth and cloud condensation nucleus activity. *Atmospheric Chemistry and Physics*, *7*(8), 1961–1971. https://doi.org/10.5194/acp-7-1961-2007

Petters, M. D., Snider, J. R., Stevens, B., Vali, G., Faloona, I., & Russell, L. M. (2006). Accumulation mode aerosol, pockets of open cells, and particle nucleation in the remote subtropical pacific marine boundary layer. *Journal of Geophysical Research*, *111*(D2), D02206. https://doi.org/10.1029/2004JD005694

Pierce, J. R., & Adams, P. J. (2009). Uncertainty in global CCN concentrations from uncertain aerosol nucleation and primary emission rates. *Atmospheric Chemistry and Physics*, *9*(4), 1339–1356. https://doi.org/10.5194/acp-9-1339-2009

Rothenberg, D., & Wang, C. (2016). Metamodeling of droplet activation for global climate models. *Journal of the Atmospheric Sciences*, *73*(3), 1255–1272. https://doi.org/10.1175/JAS-D-15-0223.1

Schulze, B. C., Charan, S. M., Kenseth, C. M., Kong, W., Bates, K. H., Williams, W., et al. (2020). Characterization of aerosol hygroscopicity over the Northeast Pacific Ocean: Impacts on prediction of CCN and stratocumulus cloud droplet number concentrations. *Earth and Space Science*, *7*(7), e2020EA001098. https://doi.org/10.1029/2020EA001098

Terai, C. R., Bretherton, C. S., Wood, R., & Painter, G. (2014). Aircraft observations of aerosol, cloud, precipitation, and boundary layer properties in pockets of open cells over the southeast Pacific. *Atmospheric Chemistry and Physics*, *14*(15), 8071–8088. https://doi.org/10.5194/acp-14-8071-2014

Twomey, S. (1977). The influence of pollution on the shortwave albedo of clouds. *Journal of the Atmospheric Sciences*, *34*(7), 1149–1152. https://doi.org/10.1175/1520-0469(1977)034<1149:tiopot>2.0.co;2

Williamson, C. J., Kupc, A., Axisa, D., Bilsback, K. R., Bui, T., Campuzano-Jost, P., et al. (2019). A large source of cloud condensation nuclei from new particle formation in the tropics. *Nature*, *574*(7778), 399–403. https://doi.org/10.1038/s41586-019-1638-9

Williamson, C. J., Kupc, A., Rollins, A., Kazil, J., Froyd, K. D., Ray, E. A., et al. (2021). Large hemispheric difference in nucleation mode aerosol concentrations in the lowermost stratosphere at mid- and high latitudes. *Atmospheric Chemistry and Physics*, *21*(11), 9065–9088. https://doi.org/10.5194/acp-21-9065-2021

Wolf, K., Ehrlich, A., Jacob, M., Crewell, S., Wirth, M., & Wendisch, M. (2019). Improvement of airborne retrievals of cloud droplet number concentration of trade wind cumulus using a synergetic approach. *Atmospheric Measurement Techniques*, *12*(3), 1635–1658. https://doi.org/10.5194/amt-12-1635-2019

Wood, R., Comstock, K. K., Bretherton, C. S., Cornish, C., Tomlinson, J., Collins, D. R., & Fairall, C. (2008). Open cellular structure in marine stratocumulus sheets. *Journal of Geophysical Research*, *113*(D12), D12207. https://doi.org/10.1029/2007JD009371

Yum, S. S., & Hudson, J. G. (2002). Maritime/continental microphysical contrasts in stratus. *Tellus B: Chemical and Physical Meteorology*, *54*(1), 61–73. https://doi.org/10.1034/j.1600-0889.2002.00268.x

Zheng, Y., Rosenfeld, D., & Li, Z. (2016). Quantifying cloud base updraft speeds of marine stratocumulus from cloud top radiative cooling. *Geophysical Research Letters*, *43*(21), 11–407. https://doi.org/10.1002/2016GL071185

19448007, 2024, 9, Downloaded from https://agupubs.onlinelibrary.wiley.com/doi/10.1029/2024GL108140 by Royal Danish Library, Wiley Online Library on [10/06/2024]. See the Terms and Conditions (https://onlinelibrary.wiley.com/terms-and-conditions) on Wiley Online Library for rules of use; OA articles are governed by the applicable Creative Commons License